Spin canting in a Dy-based single-chain magnet with dominant next-nearest-neighbor antiferromagnetic interactions

K. Bernot,[1] J. Luzon,[2] A. Caneschi,[2] D. Gatteschi,[2] R. Sessoli,[2,*] L. Bogani,[3] A. Vindigni,[4] A. Rettori,[5] and M. G. Pini[6,†]

[1]*SCR/MI-INSA Laboratory, INSA-Rennes, CS 14315, F-35043 Rennes, France*

[2]*Dipartimento di Chimica, and INSTM (UdR Firenze), Università degli Studi di Firenze, I-50019 Sesto Fiorentino (FI), Italy*

[3]*1. Physikalisches Institut, Universität Stuttgart, 70550 Stuttgart, Germany*

[4]*Laboratorium für Festkörperphysik, ETH Zürich, CH-8093 Zürich, Switzerland*

[5]*Dipartimento di Fisica, Università degli Studi di Firenze, I-50019 Sesto Fiorentino (FI), Italy*

[6]*Istituto dei Sistemi Complessi, Consiglio Nazionale delle Ricerche, I-50019 Sesto Fiorentino (FI), Italy*

(Received 13 January 2009; revised manuscript received 4 March 2009; published 15 April 2009)

We investigate theoretically and experimentally the static magnetic properties of single crystals of the molecular-based single-chain magnet of formula $[Dy(hfac)_3NIT(C_6H_4OPh)]_\infty$ comprising alternating Dy^{3+} and organic radicals. The magnetic molar susceptibility χ_M displays a strong angular variation for sample rotations around two directions perpendicular to the chain axis. A peculiar inversion between maxima and minima in the angular dependence of χ_M occurs on increasing temperature. Using information regarding the monomeric building block as well as an *ab initio* estimation of the magnetic anisotropy of the Dy^{3+} ion, this "anisotropy-inversion" phenomenon can be assigned to weak one-dimensional ferromagnetism along the chain axis. This indicates that antiferromagnetic next-nearest-neighbor interactions between Dy^{3+} ions dominate, despite the large Dy-Dy separation, over the nearest-neighbor interactions between the radicals and the Dy^{3+} ions. Measurements of the field dependence of the magnetization, both along and perpendicularly to the chain, and of the angular dependence of χ_M in a strong magnetic field confirm such an interpretation. Transfer-matrix simulations of the experimental measurements are performed using a classical one-dimensional spin model with antiferromagnetic Heisenberg exchange interaction and noncollinear uniaxial single-ion anisotropies favoring a canted antiferromagnetic spin arrangement, with a net magnetic moment along the chain axis. The fine agreement obtained with experimental data provides estimates of the Hamiltonian parameters, essential for further study of the dynamics of rare-earth-based molecular chains.

DOI: 10.1103/PhysRevB.79.134419 PACS number(s): 75.50.Xx, 75.30.Gw, 75.30.Cr, 75.10.Pq

I. INTRODUCTION

For many years, one-dimensional (1D) magnetic systems have been intensively studied owing to their simplicity. A number of sophisticated theoretical predictions have been experimentally verified as, for example: the existence of a spin gap in the excitation spectrum of integer-spin Heisenberg chains whereas half-integer spin chains have a gapless excitation spectrum (the so called Haldane conjecture[1]); the existence of a diffusive mode (the so called Villain mode[2]) in quasi-Ising $S=1/2$ antiferromagnetic spin chains; the contribution of solitons to the thermodynamic properties of easy-plane ferromagnetic[3] and antiferromagnetic[4] (AF) spin chains, with an in-plane symmetry-breaking magnetic field or anisotropy. Quasi-1D compounds, obtained by the molecular synthetic approach,[5,6] now allow the experimental investigation of dynamic phenomena that had been theoretically predicted some decades ago.[7] Such systems have been named single-chain magnets (SCMs),[8,9] by analogy with single-molecule magnets (SMMs),[10] since they show magnetic hysteresis with no evidence of three-dimensional (3D) magnetic ordering but rather due to slow dynamics of the magnetization of a pure 1D character. It was shown[9,11] that the relaxation toward thermodynamic equilibrium in these systems is driven by thermally activated single-spin flips, described in first approximation by the stochastic theory developed by Glauber[7] for the ferromagnetic 1D Ising model. The effect of introducing nonmagnetic impurities in the chain was investigated[12–14] too. The first system showing SCM behavior was the quasi-1D molecular compound of formula $[Co(hfac)_2NITPhOMe]_\infty$, where hfac is hexafluoroacetylacetonate and NITPhOMe is the nitronyl-nitroxide radical 2-PhOMe-4,4,5,5-tetramethyl-4,5-dihydro-1H-imidazolyl-1-oxil-3-oxide.[15] The repeating unit of such molecular chains is formed by two different magnetic centers, a $M^{II}(hfac)_2$ moiety containing a metal (in the present case Co^{II}), and a radical moiety that bridges the metals. The properties of this class of magnetic polymers can then be tuned, with different effects, by rationally changing either the metal or the radical moieties. In the rich field that has stemmed from this first observation, several other compounds presenting SCM behavior have been synthesized,[16–24] and evidences of quantum effects affecting the magnetization dynamics at low temperatures have also been reported.[25] A one-dimensional hysteretic behavior of the magnetization was identified also in different non-molecular structures, such as atomic Co nanowires of finite length, decorating the steps of vicinal Pt(997) surfaces.[26]

To observe Glauber dynamics two requirements are usually necessary: (i) a strong Ising-like anisotropy and (ii) a very low ratio of interchain/intrachain magnetic exchange interactions, in order for slow dynamics to be observed above the transition temperature to 3D magnetic ordering. In the framework of molecular engineering, quasi-1D chains in which the metal center is a rare-earth (RE) ion are very appealing candidates to observe a large variety of phenomena,

as REs are characterized by very different magnetic anisotropies.[27] One limiting case is constituted by molecular-based quasi-1D compounds of formula $[(Gd)(hfac)_3NITR]_\infty$ [where NIT*R* is 2-*R*-4,4,5,5-tetramethyl-4,5-dihydro-1H-imidazolyl-1-oxil-3-oxide, and *R* is ethyl (Et), isopropyl (iPr), methyl (Me), or phenyl (Ph)], where the Gd(III) ions are magnetically isotropic. In these systems helimagnetic behavior could be evidenced due to competing magnetic interactions between nearest-neighboring (NN) and next-nearest-neighboring (NNN) spin sites. When R=Et, Villain's conjecture[28] of a two-step magnetic ordering to a low-temperature helical 3D phase, through an intermediate chiral spin liquid 3D phase, was confirmed (the two transitions occurring at 1.88 K and 2.19 K, respectively).[29] When passing from isotropic Gd to Dy, which presents a strong Ising-like anisotropy, a transition to 3D magnetic order occurring at 4.4 K can be observed in $[Dy(hfac)_3NITEt]_\infty$.[30,31] However, using a bulkier $NIT(C_6H_4OPh)$ radical[32] increases the distance between chains so that SCM behavior is observed with no evidence of any 3D magnetic order down to the lowest investigated temperature (1.7 K). The two requirements (i) and (ii), necessary to observe Glauber dynamics, are thus fulfilled in $[Dy(hfac)_3NIT(C_6H_4OPh)]_\infty$. Consistently, the relaxation time τ was found[32] to follow an Arrhenius law $\tau=\tau_0 e^{\Delta/k_BT}$. In order to fully understand the rich dynamics of these quasi-1D systems,[32,33] in particular the role played by NNN interactions, a modelization of the static properties is necessary. In this paper, an accurate experimental study of the angular dependence of the single-crystal magnetization of $[Dy(hfac)_3NIT(C_6H_4OPh)]_\infty$, combined with *ab initio* estimation of the magnetic anisotropy of the Dy^{3+} ions, is presented. The static magnetic properties of the chain system are simulated by means of a classical transfer-matrix calculation, formulated for a 1D Heisenberg model with antiferromagnetic exchange coupling and noncollinear local anisotropy axes. Fine agreement with experimental data as a function of crystal orientation, temperature, and magnetic field is obtained and the Hamiltonian parameters can then be estimated. The dominant role of NNN magnetic interactions of these molecular structures, despite the large Dy-Dy separation, is clearly demonstrated. These findings are expected to be extremely important to target novel SCM dynamics in molecular compounds, and to rationalize the SCM behavior of $[Dy(hfac)_3NIT(C_6H_4OPh)]_\infty$ and the related class of compounds.[33] In particular, as the role of natural and induced defects is substantially different when competing NN and NNN interactions are present, this situation can lead to the observation of different dynamic regimes in addition to the already known ones [see Fig. 1(a) for a schematic representation of the NN and NNN magnetic interactions].

II. CRYSTAL STRUCTURE AND *AB INITIO* CALCULATIONS

Recently we investigated in detail a monomeric compound of formula $Dy(hfac)_3(NITR)_2$ where the metal ion is coordinated to the oxygen atoms of two different radicals,[34] like in the chain. In fact, we suggest that the monomer can be considered as a building block of the chain. Using angle-

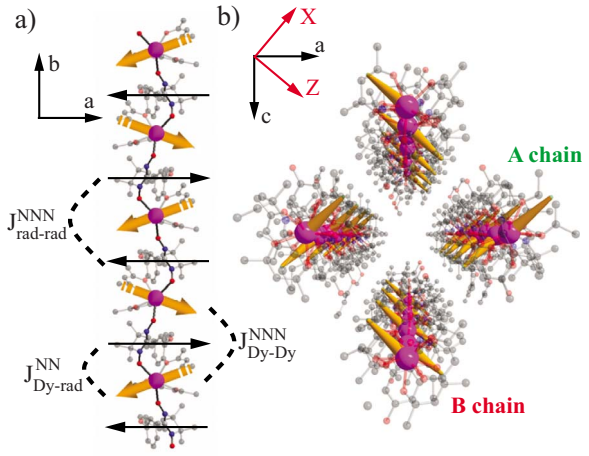

FIG. 1. (Color online) (a) Representation of the Ising axes of the Dy^{3+} ion, as gathered from *ab initio* calculations and superimposed on the chain in the *ab* plane. Thin arrows correspond to the radical spins. The three different magnetic interactions along the magnetic chain have also been represented. (b) View along the *b* crystallographic axis of the crystal packing, showing the two symmetry-related types of chains. The orientation of the *X* and *Z* axes in the *ac* plane is also represented (the *Y* axis coincides with *b*).

resolved magnetometry, the molecular magnetic-susceptibility tensor of the monomeric derivative has been reconstructed, revealing an exceptionally large Ising-type magnetic anisotropy of the Dy^{3+} ion.[34] This technique also provides the orientation of the principal magnetic axes of the monomer; the Ising axis turns out to lie in between the two radicals, almost along the binary axis of the approximate c_2 symmetry of the molecule. Moreover, the experimental findings nicely agree with *ab initio* calculations within ca. 7° deviation between the experimental and theoretical directions of the magnetization easy axis.

Here, we apply the same quantum chemistry method (CASSCF/RASSI-SO),[35] using the MOLCAS-7.0 package,[36] in order to obtain the single-ion easy-anisotropy axes of the Dy^{3+} ions in the $[Dy(hfac)_3NIT(C_6H_4OPh)]_\infty$ chain compound. In this multiconfigurational approach relativistic effects are treated in two steps, both based on the Douglas-Kroll Hamiltonian.[37] Scalar terms are included in the basis set generation and are used to determine spin-free wave functions and energies, through the use of complete active space self-consistent field (CASSCF) method. Then, spin-orbit (SO) coupling is treated with a restricted active space state interaction computation (RASSI-SO), which uses the CASSCF wave functions as the basis states. By using the resulting eigenstates of the previous method, the gyromagnetic tensor of the ground doublet Kramer's state can be computed and diagonalized in order to obtain the three main anisotropy axes and the gyromagnetic values along those axes (g_x, g_y, and g_z).

Computations are performed in a quantum cluster model considering a Dy^{3+} ion and its surrounding ligand molecules, i.e., three hfac and two NIT radicals, using the geometry determined by the x-ray structure analysis. In this cluster model several modifications have been introduced in order to reduce the large computational time: the fluorides in the hfac

TABLE I. *Ab initio* calculated energies of the eight doublets of the $^6H_{15/2}$ multiplet of the Dy^{3+} ions in the coordination environment determined from the crystallographic structure.

Doublet	E0	E1	E2	E3	E4	E5	E6	E7
Energy (K)	0	58.3	84.6	125.9	164.9	238.4	328.9	591.0

ligands have been replaced by H atoms, the NIT(C_6H_4OPh) radicals have been replaced by NIT(C_6H_5), and H atoms have been added to the external oxygen atoms of the radicals transforming them in close-shell molecules, and therefore reducing the active space of the CASSCF calculations. Despite the previous modelization, the quantum cluster would still require a large computational time due to its size. Therefore a Cholesky decomposition technique,[38] recently implemented in the MOLCAS package, is used to overcome problems arising from the large size of the two-electron integral matrix.

All the atoms were represented by basis sets of atomic natural orbitals from the ANO-RCC library, as implemented in the MOLCAS-7.0 quantum chemistry package, and the following contractions were used: [8s7p4d3f2g] for Dy, [3s2p] for O, C, and N, and [2s] for H. The CASSCF active space consisted on the Dy 4*f* orbitals, containing nine electrons in seven orbitals. The previous *ab initio* computation in the monomeric compound showed a minor role of the quadruplets and the doublets CASSCF states in the spin-orbit coupling effect on the energy levels of the $^6H_{15/2}$ ground multiplet. Therefore, only the three sextets, ^6H, ^6F, and ^6P, have been computed in three different CASSCF state average calculations, one for each of the sextets. The 21 resulting CASSCF states were introduced in a RASSI-SO state interaction in order to compute the effect of the spin-orbit coupling. The computed energies of the $^6H_{15/2}$ multiplet are listed in Table I.

The gyromagnetic factors for the ground doublet have also been evaluated and found to be $g_x=0.3$, $g_y=0.7$, and $g_z=18.7$. The computed single-ion anisotropy axis almost coincides with a binary axis in the idealized symmetry of the DyO_8 polyhedron, similarly to what observed for the monomer. The easy axis forms an angle θ of ca. 80° with respect to the *b* crystallographic axis (along the chain axis), whereas the projection of the single-ion anisotropy axis in the *ac* plane (perpendicular to the chain axis) forms an angle ϕ of ca. 50° with the *a* axis. Compared to the triclinic monomer, here the situation is complicated by the fact that the chain crystallizes in the $P2_12_12_1$ space group (N°19), $Z=4$, with three twofold screw axes as symmetry elements. The asymmetric unit contains one Dy^{3+} ion, and consequently all dysprosium atoms are symmetry related. When superimposing the Ising axis of the Dy^{3+} ion on the chain, its symmetry elements generate a canted structure as depicted in Fig. 1(a). In Fig. 1(b), a view along the chain direction (the crystallographic *b* axis) of the crystal packing of the chains is reported. As a consequence of this crystal packing, even if the chains are structurally all equivalent, they are differently oriented from the magnetic point of view. Two types of chains (A and B) are related by a 2_1 twofold screw axis (in the *ac* plane), while each of these chains is generated by its own 2_1 axis (along *b*). When analyzing the magnetic behavior of the chain, we thus have to consider not only the canted structure generated by the alternate inclination of the Ising axes with respect to the chain direction, *b*, but also the two families of chains (A and B), whose projections on the *ac* plane of the easy axis of the Dy^{3+} ions form an angle of ca. 80°.

III. MAGNETIC MEASUREMENTS

Single-crystal magnetic measurements were performed using a homemade horizontal rotator that allows, after orientation of the crystal, to measure the magnetic susceptibility along and perpendicularly to the chain axis. The morphology of the crystals, with large (101) and $(\bar{1}0\bar{1})$ faces, does not allow performing rotations along the principal crystallographic axes. We thus define a laboratory frame, (X,Y,Z), with Z corresponding to the normal to the (101) crystal face, $Y=b$, and X orthogonal to the first two. The new reference frame is thus obtained performing a rotation of the crystallographic frame, (*abc*), around *b* (the chain axis), by an angle $\alpha \approx 49.8°$ [see Fig. 1(b)].

In Fig. 2 we show the angular dependence of the ratio M/H between magnetization and field, henceforth indicated as the molar susceptibility χ_M, in three orthogonal rotations performed at 2.8 K in an external field of 1 kOe. As expected for an orthorhombic system, the crystallographic axes correspond to relative extrema. Two out of three rotations are almost identical, and display a strong angular dependence of χ_M, which has its maximum along the chain direction. The third rotation, the one around *b*, shows a very low angle-independent value of χ_M.

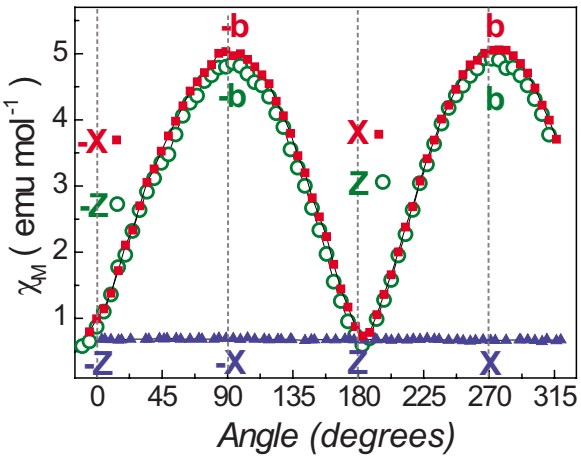

FIG. 2. (Color online) Angular variation of the molar susceptibility, χ_M, for three orthogonal rotations at 2.8 K, measured in a 1 kOe external field. Rotations were performed around X (green circles), *b* (blue triangles), and Z (red squares).

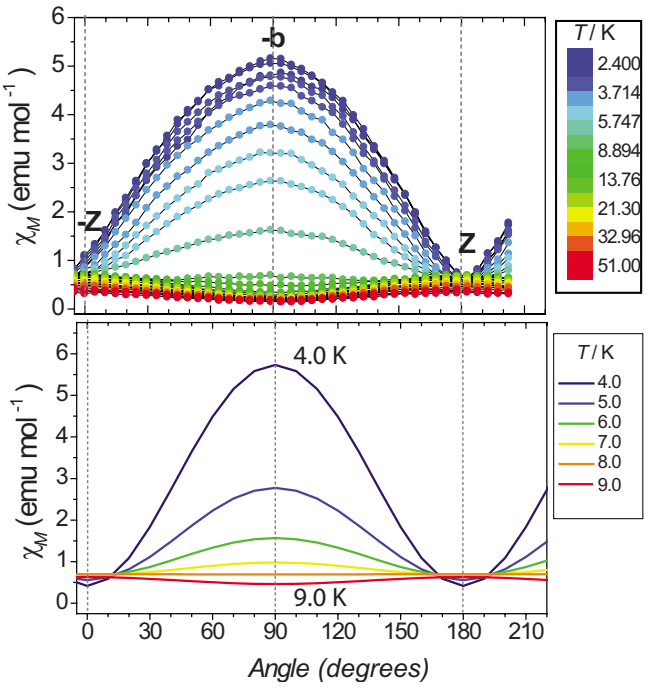

FIG. 3. (Color online) (Top) Angular variation of the molar susceptibility, $\chi_M = M/H$, for temperature T ranging from 2.4 K (blue) to 51 K (red), measured in an external magnetic field of 1 kOe. Rotations were performed around the X axis, with 0° and 180° corresponding to the field aligned perpendicularly to the chain along $-Z$ and Z, respectively, whereas, at 90°, χ_M is measured along the chain. Temperature color mapping is described on the right part of the figure. Vertical dot lines are guides to the eyes. (Bottom) Transfer-matrix simulation of the angle dependence of $\chi_M = M/H$ (with $H = 1$ kOe) when rotating around X. The classical-spin Hamiltonian, Eq. (1), and the Hamiltonian parameters specified in Sec. IV were used for the calculation. Lines of different colors refer to different temperatures.

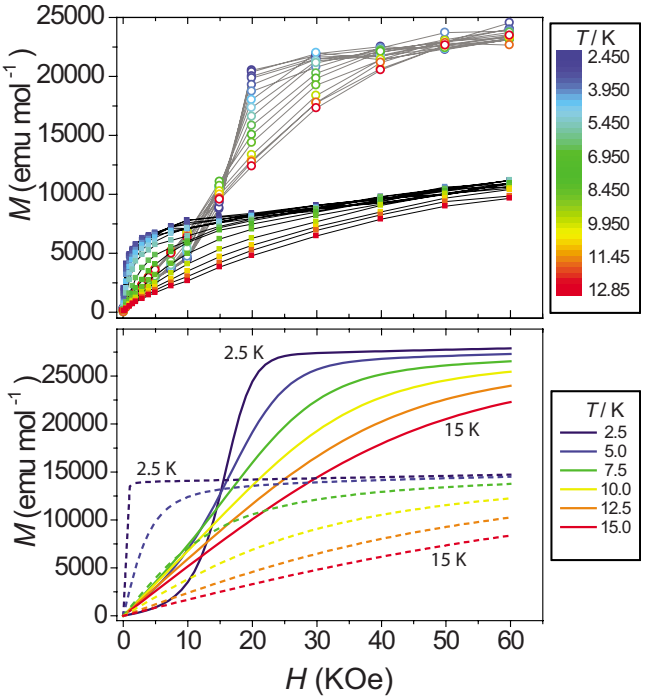

FIG. 4. (Color online) (Top) Field dependence of the magnetization along the chain (full squares) and perpendicular to the chain (along the Z axis, open circles), for temperature T ranging from 2.45 to 12.85 K. The temperature color mapping is depicted on the right. (Bottom) Transfer-matrix simulation of the field dependence of M vs H along the chain direction (dashed lines) and perpendicular to it (solid lines) obtained using the classical-spin Hamiltonian, Eq. (1), and the Hamiltonian parameters specified in Sec. IV. Lines of different colors refer to different temperatures.

The temperature-dependent magnetic behavior of $[Dy(hfac)_3NIT(C_6H_4OPh)]_\infty$ was also investigated. Measurements were performed in the 2.4–51 K temperature range, both for the angular variation in χ_M (Fig. 3) and for the field (H) dependence of the magnetization M (Fig. 4). If we consider the rotation around X reported in Fig. 3 (top) for temperatures between 2.4 and 6.5 K, the maximum of χ_M is found at 90°, thus along the chain, and the minima at 0° and 180°, i.e., perpendicularly to the chain. At 8 K, the χ_M curve has almost no angular dependence. For temperatures from 9.5 to 51 K, the maxima and minima are inverted with respect to the low-temperature curves. This is a quite spectacular and peculiar feature which, at first glance, seems troubling. However, previous investigations[34,39] give us some hints to rationalize this result:

(i) The direction of the Ising anisotropy of the Dy^{3+} ion in the monomer[34] is temperature independent in the temperature range investigated here, thus the anisotropy crossover observed around 8 K cannot be attributed solely to an electronic effect of the Dy^{3+} ions in the chain compound.

(ii) The projection of the Ising axes gathered from *ab initio* calculations and the analysis of the monomeric building block[34] of the chain structure suggests that the easy axes are not collinear.

(iii) The observed behavior (i.e., the anisotropy inversion) recalls the one encountered in $[[Mn(TPP)O_2PPh]\cdot H_2O]_\infty$ (where TPP=*meso*-tetraphenylporphyrin), a Mn^{III}-based canted antiferromagnetic SCM.[39]

It is interesting to note that similar inversions (at two different temperatures) were observed[40] in the magnetic torque curves of $TPP[Fe(Pc)(CN)_2]_2$, a molecular conductor that can be described by a one-dimensional anisotropic Heisenberg model with antiferromagnetic exchange interactions.

A scenario of a canted AF 1D structure similar to the one observed in the $[Mn(TPP)O_2PPh]\cdot H_2O$ chain[39] requires that, in the alternating Dy-radical chain under study, the NNN AF interactions dominate the NN ones [see Fig. 1(a) for a schematic representation of the NN and NNN magnetic interactions]. To confirm this hypothesis, the field dependence of the magnetization was measured. In Fig. 4 (top) we report the M vs H curves recorded along and perpendicularly to the chain. A very different shape of the curve is observed depending on whether the field is aligned along the noncompensated moment (i.e., along the chain), thus giving a rapid saturation of the magnetization, or closer to the compensated easy axes (i.e., perpendicularly to the chain), providing a sort of metamagnetic transition when the magnetic field overwhelms the antiferromagnetic interaction (see Sec. IV for quantitative details).

The rapid saturation of the component along the chain observed at 3 K, with a plateau corresponding to ca 10 000 emu mol^{-1}($\approx 1.8\mu_B$), is the typical behavior expected for a weak ferromagnet (WF)—indeed in this case a 1D WF—along the direction of the noncompensated moments. Perpendicularly to the chain, and more precisely along the Z axis, the magnetization is almost linear at low field, but shows a rapid increase around 15 kOe and saturation at larger fields, almost 22 000 emu mol^{-1}($\approx 4.1\mu_B$).

Interestingly, the step in the magnetization perpendicular to the chain becomes smoother when temperature is increased, and finally disappears for temperatures above 10 K, when the weak AF interaction becomes negligible and the anisotropy of the sample is driven by the single-ion anisotropy of the Dy^{3+}. When the field is applied along the chain direction, i.e., the direction of the noncompensated moment, a more regular behavior is observed, as the initial susceptibility monotonously decreases with increasing temperatures.

This feature sheds some light on the quite unique behavior of the whole family of lanthanide-based SCMs.[32,33] Magnetization curves recorded on the 4f-based SCM family always display steps at relatively high field, and a trend was observed along the lanthanide series.[32,33] In fact, the position of the step is explained by the simultaneous presence of an anisotropic center (providing the anisotropic canted structure) and of an AF interaction along the chain. Hence, the stronger is the intrachain magnetic interaction, the higher is the field needed to compensate this interaction, shifting the step toward higher fields.

This allows concluding that, in the $[Dy(hfac)_3NIT(C_6H_4OPh)]_\infty$ SCM under study:

(i) Antiferromagnetic interaction between Dy^{3+} ions is present. Due to this fact, the magnetization components perpendicular to the chain direction cancel out at low temperature and low field, while they become favored at higher temperatures.

(ii) The high-temperature hard axis becomes the easy axis at low temperature because noncompensation of the canted spins occurs.

(iii) The anisotropy inversion is visible around 9 K, suggesting a relatively weak intrachain exchange interactions, as expected in compounds involving tripositive lanthanides.

If we now compare the observed magnetization values for the chain and the monomer derivative, a first saturation $M_{sat} \approx 58\,000$ emu mol^{-1}($\approx 11\mu_B$) has been observed along the easy axis of the monomer.[34] At a first level of approximation we can neglect the radical contribution, which is much smaller than that given by the paramagnetic ions; moreover, the "radical" sublattice is on itself experiencing AF interactions mediated by the lanthanide ion and is also frustrated due to the sizeable AF NNN interaction between Dy^{3+} spins (see Sec. IV).[34] This allows providing a rough estimation of the angle, θ, formed by the easy axis of each Dy^{3+} center with the chain axis, b. In fact, comparing the aforementioned saturation value ($\approx 58\,000$ emu mol^{-1}) with the rapid saturation one (≈ 8000 emu mol^{-1}) reached when the field is applied along the chain, yields $\theta = \cos^{-1}(8000/58000) \approx 82°$. This value is consistent with the results of the *ab initio* calculations.

As for the magnetization curve measured perpendicularly to the chain, the field was applied aligned along Z. Considering the direction of the local easy axes predicted by the *ab initio* calculations [see Fig. 1(b)], the applied field is almost parallel to the projection of these axes on the *ac* plane for type B chains, whereas it is almost perpendicular to type A chains. For the two symmetry-related families of chains, A and B, the projections of the local easy axes on the *ac* plane are almost reciprocally perpendicular but, remarkably, this is a fully accidental coincidence rather than a symmetry-imposed result. Therefore, as schematically represented in Fig. 5, the applied field can compete with the AF interaction inside the chain of type B whereas it has no effect on the other family (A), where Dy^{3+} spins remain antiferromagnetically coupled. Thus, only one chain type is contributing to the magnetization, which should approach a value $M = (\frac{1}{2})58\,000 \sin\theta$ (that is, $M \approx 28\,700$ emu mol^{-1}), not very far from the experimental value. Despite the fact that these figures can be only taken as indicative, given the rough approximation of neglecting the radical contribution, such saturation values for the magnetization are in agreement with our prediction about the orientation of the local easy axes, based on the *ab initio* calculations.

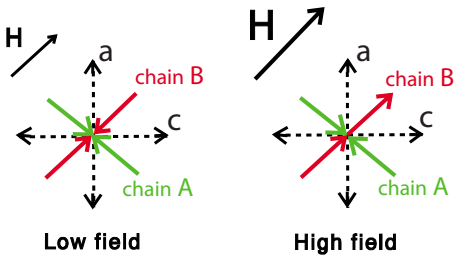

FIG. 5. (Color online) Influence of an applied magnetic field in the *ac* plane on the orientation of the magnetic moments of neighboring Dy ions of the two types of chains (A and B).

A further confirmation of the correctness of this hypothesis can be afforded by performing, at low temperature, a rotation around b (the chain axis) under an external field of 30 kOe: i.e., a field strong enough to be capable of distinguishing the different projections of the Ising axes in the *ac* plane by overcoming the AF interaction. From Fig. 6 (top) one can clearly see that contrarily to what observed at low field, χ_M is now angle dependent, with a very peculiar behavior with large maxima and a roughly 90° periodicity. It should be noticed that:

(i) The absolute maxima are observed along the crystallographic axes a and c, and not along the directions where the projections of the local axes fall.

(ii) The data show a secondary periodical structure of smaller maxima shifted by an angle of ca. 45°.

As a final remark, we notice that the maxima observed in Fig. 6 (top) along a and c are not strictly equivalent, but the direction c appears to be favored. In Sec. IV we will show that this feature can be interpreted as due to a slight (but appreciable) departure from orthogonality of the projection on the *ac* plane of the local easy axis of Dy^{3+} ions belonging to the two symmetry-related chain families, A and B, as indeed predicted by *ab initio* calculations.

We have also checked the temperature dependence of the anisotropy when rotating at high field around the chain axis,

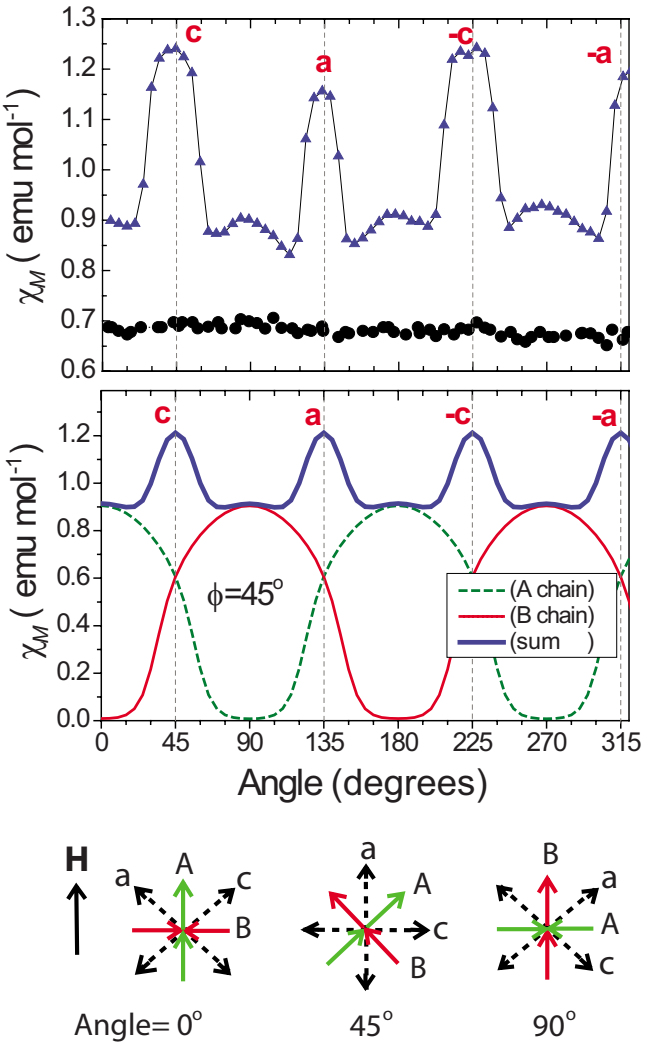

FIG. 6. (Color online) (Top) Angular variation of the molar susceptibility ($\chi_M = M/H$) for the rotations around the chain axis b at 2.5 K, measured in a 30 kOe external field (blue triangles) or in a 1 kOe external field (black triangles). (Center) Transfer-matrix simulation of M/H vs angle at 2.5 K in a field of 30 kOe, showing the contribution from each chain type (A and B), as well as their sum. The classical-spin Hamiltonian, Eq. (1), and the Hamiltonian parameters specified in Sec. IV were used for the calculation. Perfect orthogonality $2\phi = 90°$ between the projections on the ac plane of the easy axes of the two chain families A and B was assumed. (Bottom) Schematic representation of the corresponding spin configurations.

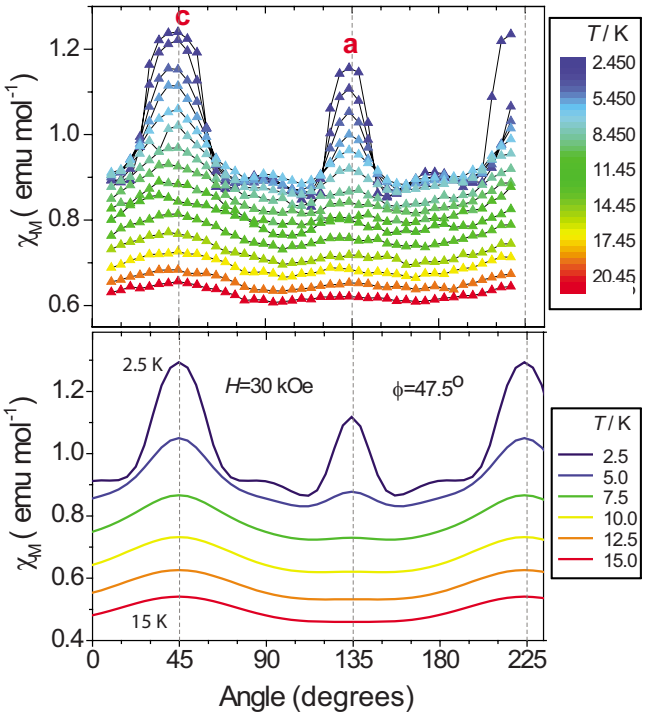

FIG. 7. (Color online) (Top) Angular variation of the susceptibility $\chi_M = M/H$ from 2.45 K (blue) to 20.45 K (red) measured in a 30 kOe external field. Rotations were performed around the chain axis b as defined in the text. Color mapping is described on the right part of the figure. Solid lines are guides to the eyes. (Bottom) Transfer matrix simulation of $\chi_M = M/H$ vs angle, at selected temperatures in a field of 30 kOe. The classical-spin Hamiltonian, Eq. (1), and the Hamiltonian parameters specified in Sec. IV were used for the calculation. Notice that, with respect to Fig. 6 (center), a slight deviation from perfect orthogonality between the two chain families was assumed, thus accounting for asymmetry in the height of the major peaks.

b (see Fig. 7, top). The results show that the behavior is strongly temperature dependent. Since in this temperature range the Dy^{3+} anisotropy of the monomeric constituent units of the chain does not change, these data confirm the key role played by the exchange interaction, suggesting an order of magnitude of the AF interaction of a few Kelvins (see Sec. IV for a more detailed discussion).

IV. THEORY AND DISCUSSION

In order to interpret the measurements of the static magnetic properties of the chain, we model both A and B chains with a classical-spin Hamiltonian

$$\mathcal{H} = -\sum_{\mathrm{I}} \left\{ J\mathbf{S}(\mathrm{I}) \cdot \mathbf{S}(\mathrm{I}+1) + D[S_{z_{\mathrm{I}}'}(\mathrm{I})]^2 + \mu_0 \sum_{\alpha,\beta} H_\alpha g_{\alpha\beta} S_\beta(\mathrm{I}) \right\}, \tag{1}$$

where μ_0 is the Bohr magneton and $\alpha, \beta = X, Y, Z$ denote Cartesian components in the crystallographic frame (a, b, and c), while the subscript z_{I}' denotes the spin component along a local anisotropy axis, varying with lattice site I. In the sum, only the Dy centers are considered for the reasons given below. The AF exchange interaction ($J<0$) is considered isotropic, while the anisotropy is introduced through a single-ion term ($D>0$) favoring local $\mathbf{z}_{\mathrm{I}}'$ axes, which are different for even and odd sites, and in the Landé tensor ($g_{\alpha\beta}$). In a local reference frame, the Landé tensor is assumed to have only diagonal components, $g_\parallel$ and $g_\perp$ (where parallel and perpendicular refer to the local axis $\mathbf{z}_{\mathrm{I}}'$). Since spin Hamiltonian (1) is classical, the spin modulus S does not matter (its effect can be taken into account by the parameters J, D, and g's). For an easy comparison with the calculation performed for the monomer,[34] we will assume $S = 1/2$. Notice that the classical nature of the spins allows the inclusion of single-ion anisotropy even in this case.[34] Concerning the

neglect of the radicals, we note that their anisotropy is very low compared to the Dy^{3+} one, and the Dy-radical interaction is necessarily frustrated since the interaction between the Dy^{3+} ions is antiferromagnetic. As a first approximation, the system can thus be considered as the superposition of two independent one-dimensional magnetic lattices, one formed by the Dy^{3+} ions (with magnetic anisotropy) and the other by the radicals (magnetically isotropic). At low temperatures, the contribution of the "radical" lattice is expected to be very small because of the relatively strong NNN antiferromagnetic interaction between radicals.[34]

Using a transfer-matrix method,[41] the static magnetic properties of 1D classical-spin model (1) can be exactly expressed in terms of the eigenvalues and eigenvectors of a real positive-definite matrix (see the Appendix for details). In this way, starting from certain values of the Hamiltonian parameters, we were able to numerically simulate the static magnetic behavior of the real chain compound. The simulation procedure started from placing the local easy axes at $\theta = 75°$ from the b axis and its projection on the ac plane at $\phi = \pm 45°$ from a. The other Hamiltonian parameters used for the simulation were $J = -24$ K, $D = 160$ K, $g_{\parallel} = 21$, and $g_{\perp} = 4$, where parallel and perpendicular refer to the local $\mathbf{z}_1'$ axis. The contributions from the two families of chains were then summed up. In Fig. 3 (bottom) we report a simulation of the quantity M/H, calculated for different temperatures when rotating along X, to be compared with the measured dc susceptibility in Fig. 3 (top). The susceptibility presents a maximum along b and a minimum along Z for $T < 8$ K, while the trend is reversed for $T > 8$ K. Thus, the anisotropy inversion observed at $T = 8.5$ K on the experimental data in Fig. 3 (top) is nicely reproduced.

The field dependence of the magnetization at selected temperatures, both for H parallel and perpendicular to the chain, was simulated using the same Hamiltonian parameters: see Fig. 4 (bottom). The measured overall behavior of Fig. 4 (top) was reproduced, although a more quantitative comparison was prevented by the neglect of the radical contribution in adopted model (1).

In particular, a relationship between the field at which a rapid increase in the magnetization perpendicular to the chain is observed and the transfer-matrix-computation parameters can be deduced by simple arguments. Without loss of generality, we assume that spins are essentially constrained to be oriented along their local anisotropy axes at low temperatures and consider an applied field lying on the ac plane at $\phi = +45°$ from a. This implies that the Zeeman energy of half of the spins is frustrated (the $\mathbf{S}^{\mathrm{II}}$-spin sublattice with the notation of the Appendix). The flip of such spins lowers the Zeeman energy per spin by a factor $\Delta E_{\mathrm{Zeeman}} = 2S g_{\parallel} \mu_B H \sin\theta$. On the other hand, the corresponding increase in the exchange energy per spin is $\Delta E_{\mathrm{exch}} = 4S^2 |J \cos(2\theta)|$. The reversal of such a sublattice is expected to occur when these two energies are equal, i.e., at the field $H_{\mathrm{flip}} = \frac{2S|J\cos(2\theta)|}{g_{\parallel}\mu_B \sin\theta} = 15.25$ kOe. These naïve energy considerations give the correct value for the "jump" field [see Fig. 4 (bottom)], the effect of temperature being solely that of rounding the step in the magnetization curve.

Under quite general conditions,[42] the correlation length ξ of anisotropic classical-spin chains behaves asymptotically at low temperatures as $\xi \sim \exp(\frac{\Delta E_{\mathrm{exch}}}{2k_B T})$. Consequently, for $T \geq \frac{\Delta E_{\mathrm{exch}}}{2k_B}$, both families of spin chains are expected to lose their genuine 1D character and respond to a field as independent anisotropic paramagnetic centers. Again, the order of magnitude of $\frac{\Delta E_{\mathrm{exch}}}{2k_B} = 10.4$ K matches with the temperature at which the anisotropy inversion was observed.

The rotation around the chain axis, b, of the molar susceptibility was also simulated in a strong external field ($H = 30$ kOe), and the contributions from each family of chains (A and B) are reported in Fig. 6 (center), along with their sum. A qualitative explanation of the observed behavior can be obtained by looking in detail at the effect of the field when it is applied at different angles in the ac plane: see Fig. 6 (bottom). When the field is along a (or c), it lies at nearly 45° from the easy axis of both families of chains. Even if a smaller component of the field (indeed proportional to cos 45°) acts on the magnetic moments, this is still enough to overcome the AF interaction. This is for example represented by the arrows at Angle=45° in Fig. 6 (bottom). Given the large anisotropy of Dy^{3+} in this environment, the magnetic moments remain aligned along their easy axis, and only the weak intrachain AF interaction is overcome. The largest magnetization value we can measure is therefore reduced to $M_{\mathrm{sat}} \sin 75° \cos 45° \approx 39\,600$ emu mol^{-1}, not too far from the observed value ($\approx 37\,500$ emu mol^{-1}). It is evident that each chain type gives a contribution with a periodicity of 180° so that, owing to the accidental orthogonality between the two families A and B, the overall periodicity is ≈90°.

Finally, in order to simulate the asymmetry in the height of the major peaks displayed in Fig. 6 (top), the hypothesis of a perfect orthogonality between the projections of the two chain types, A and B, was released. In Fig. 7 (bottom) the angular variation in χ_M at selected temperatures, calculated assuming an angle ϕ between a and the projection of the local easy axes in the ac plane for the A-type chain slightly larger than 45°, is reported. The fine agreement with experimental data (see Fig. 7, top) proves that the different height of the major peaks at 45° and 135° can be attributed to nonperfect orthogonality. Interestingly, even the minor maxima between two main maxima are reproduced at sufficiently low temperatures.

V. CONCLUSIONS

In conclusion, we have performed a thorough experimental and theoretical investigation to rationalize the complex magnetic behavior of the Dy-based SCM $[Dy(hfac)_3NIT(C_6H_4OPh)]_{\infty}$. By means of angle-resolved magnetometry the magnetic anisotropy of this complex system has been accurately determined and it has been possible to evidence a peculiar "anisotropy-inversion" phenomenon, in which the easy and hard axes of the magnetization of the system swap when rising the temperature. These features could be fully explained, with excellent agreement between theory and experiments, using a combined theoretical approach in which the single RE-ion anisotropy is described at the quantum-chemical level while the thermodynamic properties of the whole system of coupled ions are computed with

a classical-spin Hamiltonian. This combined theoretical strategy is mandatory to tackle the complexity of anisotropic magnetic molecular materials, often characterized by a low-symmetry environment of the magnetic centers. The rich magnetic behavior of $[Dy(hfac)_3NIT(C_6H_4OPh)]_\infty$ was well reproduced by the model calculations that highlighted the presence of two sets of noninteracting parallel chains, with their projections mutually tilted by about 90°. Accordingly, the metamagnetic transition inside each symmetry-related family of chains could be addressed independently. The combined approach has also allowed quantifying the sign, magnitude and role of NNN interactions between Dy^{3+} ions. Despite the large distances between the REs (>8 Å), the overall behavior is actually dominated by this antiferromagnetic NNN exchange pathway, which gives rise to the very rich magnetic behavior observed. The same evidence was previously reported for isotropic Gd ions. The present finding shows that NNN are more common than believed so far and may induce a critical revision of the description of the magnetic properties of polynuclear compounds. The present study may thus represent a methodological guide line to rationalize the magnetic properties of RE-based SCMs as well as other extremely complex behaviors displayed by molecular materials in general. To the aim of understanding the dynamic behavior of RE-based SCMs, the obtained information represents a fundamental preliminary step; from the knowledge that competing NN and NNN interactions are present, for instance, one can reasonably expect the observation of particular dynamic regimes. For instance, we expect the effect of natural and induced defects to be substantially different than the already known cases in which only NN interactions are present.[12–14] As an example, preliminary results indicate that, while the contribution of the radicals to the static properties is almost negligible, they actively contribute to the correlation length even when the Dy^{3+} ions are partially substituted by diamagnetic ions. In this sense, by doping with diamagnetic ions the controlled interaction between segments of chains can be tuned, thus allowing a further form of engineering of the dynamic properties.

ACKNOWLEDGMENTS

We acknowledge financial support from the NEMAGMANET (Grant No. FP6-NMP3-CT-2005-515767), the Seventh Framework Programme of EC (Grant No. FP7-PIEF-GA-2008-220498), and the German DFG (Grant No. SPP1137).

APPENDIX: TRANSFER-MATRIX METHOD

In this appendix, we briefly describe the transfer-matrix method, which allows the determination, at any nonzero temperature, of the static properties of a one-dimensional model of classical spins in terms of the eigenvalues and eigenfunctions of a real positive-definite matrix. Here the method will be applied in the thermodynamic limit, but it can be reformulated also to treat the case of a finite system with open or periodic boundary conditions.

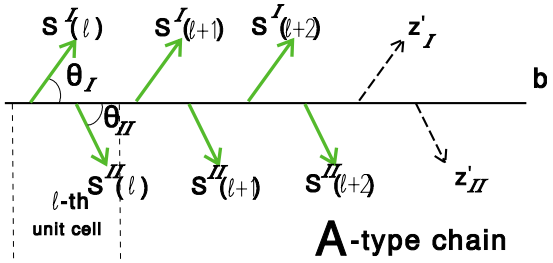

FIG. 8. (Color online) Canted ground state of the spins of a single chain of type A, described by Hamiltonian (1). For each unit cell l, there are two spins (thick, green arrows, representing Dy^{3+} ions) that belong to two different sublattices, I and II, with different local axes $\mathbf{z}'_{\mathrm{I}}$ and $\mathbf{z}'_{\mathrm{II}}$ (thin, dashed arrows).

It is worth noticing that the method is exact: the only approximation is that the spins are considered as classical vectors. Since the method requires an integration over the unit sphere surface to be discretized, numerical errors are significant only at very low temperatures, where the integrand presents strong variations over the integration domain. However, the accuracy of the method can be improved at will by using a greater number of integration points.

Following Pandit and Tannous,[41] we consider a single magnetic chain with *two sublattices*, I and II (not to be confused with the *two families* of chains related by "accidental" orthogonality, A and B).

To fix ideas, let us consider a single A-type chain: in the lth unit cell, there are two spins, $\mathbf{S}^{\mathrm{I}}(l)$ and $\mathbf{S}^{\mathrm{II}}(l)$, characterized by two different local axes, $\mathbf{z}'_{\mathrm{I}}$ and $\mathbf{z}'_{\mathrm{II}}$, forming equal angles ($\theta_{\mathrm{I}}=\theta_{\mathrm{II}}=75°$, see Fig. 8) with the chain axis b and their projections in the ac plane differing by 180° ($\phi_{\mathrm{I}}=45°$, $\phi_{\mathrm{II}}=225°$) with the a axis.

The Hamiltonian of the chain can be rewritten, as in Ref. 41, in the form

$$\mathcal{H}=\sum_{l=1}^{N}\{V_1[\mathbf{S}^{\mathrm{I}}(l),\mathbf{S}^{\mathrm{II}}(l)]+V_2[\mathbf{S}^{\mathrm{II}}(l),\mathbf{S}^{\mathrm{I}}(l+1)]\}, \quad \text{(A1)}$$

where the total number of spins, in the single A-type chain considered, is $2N$ because there are two spins per each unit cell ($l=1,\ldots,N$). In our case, V_1 and V_2 take the forms ($\alpha,\beta=X,Y,Z$)

$$V_1[\mathbf{S}^{\mathrm{I}}(l),\mathbf{S}^{\mathrm{II}}(l)]=-J\mathbf{S}^{\mathrm{I}}(l)\cdot\mathbf{S}^{\mathrm{II}}(l)-\frac{D}{2}\{[S^{\mathrm{I}}_{z'_{\mathrm{I}}}(l)]^2+[S^{\mathrm{II}}_{z'_{\mathrm{II}}}(l)]^2\}$$
$$-\frac{1}{2}\mu_0\sum_{\alpha,\beta}H_\alpha\{g^{\mathrm{I}}_{\alpha\beta}S^{\mathrm{I}}_\beta(l)+g^{\mathrm{II}}_{\alpha\beta}S^{\mathrm{II}}_\beta(l)\}, \quad \text{(A2)}$$

$$V_2[\mathbf{S}^{\mathrm{II}}(l),\mathbf{S}^{\mathrm{I}}(l+1)]=-J\mathbf{S}^{\mathrm{II}}(l)\cdot\mathbf{S}^{\mathrm{I}}(l+1)$$
$$-\frac{D}{2}\{[S^{\mathrm{II}}_{z'_{\mathrm{II}}}(l)]^2+[S^{\mathrm{I}}_{z'_{\mathrm{I}}}(l+1)]^2\}$$
$$-\frac{1}{2}\mu_0\sum_{\alpha,\beta}H_\alpha\{g^{\mathrm{II}}_{\alpha\beta}S^{\mathrm{II}}_\beta(l)+g^{\mathrm{I}}_{\alpha\beta}S^{\mathrm{I}}_\beta(l+1)\}. \quad \text{(A3)}$$

Clearly, in the previous equations one has to take into account that the crystallographic (laboratory) frame (X,Y,Z) and the local frame (x',y',z') are related by a rotation, so that for the I sublattice one has

$$S^{\mathrm{I}}_{z'_{\mathrm{I}}} = \sin\theta_{\mathrm{I}}\cos\phi_{\mathrm{I}} S^{\mathrm{I}}_X + \sin\theta_{\mathrm{I}}\sin\phi_{\mathrm{I}} S^{\mathrm{I}}_Y + \cos\theta_{\mathrm{I}} S^{\mathrm{I}}_Z, \quad \text{(A4)}$$

$$g^{\mathrm{I}}_{XX} = g_{\perp}(\cos^2\theta_{\mathrm{I}}\cos^2\phi_{\mathrm{I}} + \sin^2\phi_{\mathrm{I}}) + g_{\parallel}\sin^2\theta_{\mathrm{I}}\cos^2\phi_{\mathrm{I}}, \quad \text{(A5)}$$

$$g^{\mathrm{I}}_{XY} = (g_{\parallel} - g_{\perp})\sin^2\theta_{\mathrm{I}}\cos\phi_{\mathrm{I}}\sin\phi_{\mathrm{I}}, \quad \text{(A6)}$$

$$g^{\mathrm{I}}_{XZ} = (g_{\parallel} - g_{\perp})\cos\theta_{\mathrm{I}}\sin\theta_{\mathrm{I}}\cos\phi_{\mathrm{I}}, \quad \text{(A7)}$$

$$g^{\mathrm{I}}_{YX} = g^{\mathrm{I}}_{XY}, \quad \text{(A8)}$$

$$g^{\mathrm{I}}_{YY} = g_{\perp}(\cos^2\theta_{\mathrm{I}}\sin^2\phi_{\mathrm{I}} + \cos^2\phi_{\mathrm{I}}) + g_{\parallel}\sin^2\theta_{\mathrm{I}}\sin^2\phi_{\mathrm{I}}, \quad \text{(A9)}$$

$$g^{\mathrm{I}}_{YZ} = (g_{\parallel} - g_{\perp})\cos\theta_{\mathrm{I}}\sin\theta_{\mathrm{I}}\sin\phi_{\mathrm{I}}, \quad \text{(A10)}$$

$$g^{\mathrm{I}}_{ZX} = g^{\mathrm{I}}_{XZ}, \quad \text{(A11)}$$

$$g^{\mathrm{I}}_{ZY} = g^{\mathrm{I}}_{XZ}, \quad \text{(A12)}$$

$$g^{\mathrm{I}}_{ZZ} = g_{\perp}\sin^2\theta_{\mathrm{I}} + g_{\parallel}\cos^2\theta_{\mathrm{I}}, \quad \text{(A13)}$$

and similar equations for the other (II) sublattice.

The partition function $Z=\mathrm{Tr}\, e^{-\beta\mathcal{H}}$ can be written as

$$Z = \int d\mathbf{S}^{\mathrm{I}}(1)\int d\mathbf{S}^{\mathrm{II}}(1)\cdots\int d\mathbf{S}^{\mathrm{I}}(N)\int d\mathbf{S}^{\mathrm{II}}(N) \times e^{-\beta V_1[\mathbf{S}^{\mathrm{I}}(1),\mathbf{S}^{\mathrm{II}}(1)]}e^{-\beta V_2[\mathbf{S}^{\mathrm{II}}(1),\mathbf{S}^{\mathrm{I}}(2)]}\cdots \times e^{-\beta V_1[\mathbf{S}^{\mathrm{I}}(N),\mathbf{S}^{\mathrm{II}}(N)]}e^{-\beta V_2[\mathbf{S}^{\mathrm{II}}(N),\mathbf{S}^{\mathrm{I}}(1)]}, \quad \text{(A14)}$$

where periodic boundary conditions, $\mathbf{S}^{\mathrm{I}}(N+1)=\mathbf{S}^{\mathrm{I}}(1)$, were assumed.[41] A symmetric positive-definite kernel $\mathcal{T}$ can now be defined,

$$\mathcal{T}[\mathbf{S}^{\mathrm{I}}(l),\mathbf{S}^{\mathrm{I}}(l+1)] = \int d\mathbf{S}^{\mathrm{II}}(l) \times e^{-\beta V_1[\mathbf{S}^{\mathrm{I}}(l),\mathbf{S}^{\mathrm{II}}(l)]}e^{-\beta V_2[\mathbf{S}^{\mathrm{II}}(l),\mathbf{S}^{\mathrm{I}}(l+1)]}. \quad \text{(A15)}$$

Denoting by λ_n and $\Psi_n[\mathbf{S}^{\mathrm{I}}(l)]$ the eigenvalues and corresponding eigenfunctions of Eq. (A15)

$$\int d\mathbf{S}^{\mathrm{I}}(l+1)\mathcal{T}[\mathbf{S}^{\mathrm{I}}(l),\mathbf{S}^{\mathrm{I}}(l+1)]\Psi_n[\mathbf{S}^{\mathrm{I}}(l+1)] = \lambda_n\Psi_n[\mathbf{S}^{\mathrm{I}}(l)], \quad \text{(A16)}$$

one has that the largest eigenvalue λ_1 is always nondegenerate, and the eigenfunctions satisfy the two conditions,

$$\mathcal{T}[\mathbf{S}^{\mathrm{I}}(l),\mathbf{S}^{\mathrm{I}}(l+1)] = \sum_n \lambda_n \times \Psi^*_n[\mathbf{S}^{\mathrm{I}}(l)]\Psi_n[\mathbf{S}^{\mathrm{I}}(l+1)], \quad \text{(A17)}$$

$$\int d\mathbf{S}^{\mathrm{I}}(l)\Psi^*_n[\mathbf{S}^{\mathrm{I}}(l)]\Psi_m[\mathbf{S}^{\mathrm{I}}(l)] = \delta_{n,m} \quad \text{(A18)}$$

of completeness and orthonormality, respectively. Now, using first Eq. (A17) to expand the kernel of Eq. (A15), and then exploiting Eq. (A18), the partition function Z can be rewritten as

$$Z = \int d\mathbf{S}^{\mathrm{I}}(1)\int d\mathbf{S}^{\mathrm{I}}(2)\cdots\int d\mathbf{S}^{\mathrm{I}}(N) \times \mathcal{T}[\mathbf{S}^{\mathrm{I}}(1),\mathbf{S}^{\mathrm{I}}(2)]\mathcal{T}[\mathbf{S}^{\mathrm{I}}(2),\mathbf{S}^{\mathrm{I}}(3)]\cdots\mathcal{T}[\mathbf{S}^{\mathrm{I}}(N),\mathbf{S}^{\mathrm{I}}(1)] = \sum_{n=1}^{\infty}(\lambda_n)^N \to \lambda_1^N, \quad \text{(A19)}$$

where the largest eigenvalue λ_1 dominates in the thermodynamic limit $N\to\infty$. Using a similar procedure, the crystallographic components $(\alpha=X,Y,Z)$ of the magnetization per site on the I sublattice can be expressed, for $N\to\infty$, as

$$\langle S^{\mathrm{I}}_{\alpha}\rangle = \int d\mathbf{S}^{\mathrm{I}}\Psi^*_1(\mathbf{S}^{\mathrm{I}})S^{\mathrm{I}}_{\alpha}\Psi_1(\mathbf{S}^{\mathrm{I}}). \quad \text{(A20)}$$

In order to calculate the same quantities on the other (II) sublattice of the single (A-type) chain considered, one defines another symmetric positive-definite kernel $\mathcal{U}$ and another integral equation, respectively,

$$\mathcal{U}[\mathbf{S}^{\mathrm{II}}(l),\mathbf{S}^{\mathrm{II}}(l+1)] = \int d\mathbf{S}^{\mathrm{I}}(l+1) \times e^{-\beta V_2[\mathbf{S}^{\mathrm{II}}(l),\mathbf{S}^{\mathrm{I}}(l+1)]}e^{-\beta V_1[\mathbf{S}^{\mathrm{I}}(l+1),\mathbf{S}^{\mathrm{II}}(l+1)]}, \quad \text{(A21)}$$

$$\int d\mathbf{S}^{\mathrm{II}}(l)\Phi_n[\mathbf{S}^{\mathrm{II}}(l)]\mathcal{U}[\mathbf{S}^{\mathrm{II}}(l),\mathbf{S}^{\mathrm{II}}(l+1)] = \lambda_n\Phi_n[\mathbf{S}^{\mathrm{II}}(l+1)]. \quad \text{(A22)}$$

Notice that the eigenvalues of Eqs. (A22) and (A16) are equal so that the partition function Z is the same, while the eigenfunctions are different. Similarly to Eq. (A20), the crystallographic components $(\alpha=X,Y,Z)$ of the magnetization per site on the II sublattice can be expressed, in the thermodynamic limit, as

$$\langle S^{\mathrm{II}}_{\alpha}\rangle = \int d\mathbf{S}^{\mathrm{II}}\Phi^*_1(\mathbf{S}^{\mathrm{II}})S^{\mathrm{II}}_{\alpha}\Phi_1(\mathbf{S}^{\mathrm{II}}). \quad \text{(A23)}$$

For small applied fields, the crystallographic components $(\alpha=X,Y,Z)$ of the molar susceptibility χ^{α}_M for the single (A-type) chain considered are then obtained from Eqs. (A23) as

$$\chi^{\alpha}_M = \frac{1}{2}N_0\mu_0\frac{1}{H^{\alpha}}\sum_{\beta}(g^{\mathrm{I}}_{\alpha\beta}\langle S^{\mathrm{I}}_{\beta}\rangle + g^{\mathrm{II}}_{\alpha\beta}\langle S^{\mathrm{II}}_{\beta}\rangle), \quad \text{(A24)}$$

where N_0 is Avogadro's number.

The total susceptibility, to be compared with experimental data, is then obtained by repeating the calculation for a chain belonging to the other family,[43] i.e., B (related to A by "accidental" orthogonality), and then averaging over the two contributions.

With regard to the details of numerical calculations, following Pandit and Tannous,[41] the integrals over the surface of a sphere in Eqs. (A16) and (A22) were approximated by using McLaren's 72-points 14th-degree formula. Thus, the eigenvalues and eigenfunctions of the two integral Eqs. (A16) and (A22) were obtained solving a (72×72)-matrix eigenvalue problem by standard numerical methods.[44] Because of discretization, errors are significant only at very low temperatures, where the integrands in Eqs. (A16) and (A22) present strong variations over the integration domains. However, the accuracy of the method can be improved by using a greater number of integration points.

*roberta.sessoli@unifi.it
†mariagloria.pini@fi.isc.cnr.it

[1] F. D. M. Haldane, Phys. Lett. **93A**, 464 (1983); Phys. Rev. Lett. **50**, 1153 (1983).
[2] J. Villain, Physica B & C **79**, 1 (1975).
[3] H. J. Mikeska, J. Phys. C **11**, L29 (1978).
[4] H. J. Mikeska, J. Phys. C **13**, 2913 (1980).
[5] A. Caneschi, D. Gatteschi, R. Sessoli, and P. Rey, Mol. Cryst. Liq. Cryst. **176**, 329 (1989).
[6] S. J. Blundell and F. L. Pratt, J. Phys.: Condens. Matter **16**, R771 (2004).
[7] R. J. Glauber, J. Math. Phys. **4**, 294 (1963).
[8] L. Bogani, A. Vindigni, R. Sessoli, and D. Gatteschi, J. Mater. Chem. **18**, 4750 (2008), and references therein.
[9] C. Coulon, H. Miyasaka, and R. Clerac, Struct. Bonding (Berlin) **122**, 163 (2006).
[10] D. Gatteschi, R. Sessoli, and J. Villain, *Molecular Nanomagnets* (Oxford University Press, Oxford, UK, 2006).
[11] A. Caneschi, D. Gatteschi, N. Lalioti, C. Sangregorio, R. Sessoli, G. Venturi, A. Vindigni, A. Rettori, M. G. Pini, and M. A. Novak, Europhys. Lett. **58**, 771 (2002).
[12] L. Bogani, A. Caneschi, M. Fedi, D. Gatteschi, M. Massi, M. A. Novak, M. G. Pini, A. Rettori, R. Sessoli, and A. Vindigni, Phys. Rev. Lett. **92**, 207204 (2004).
[13] L. Bogani, R. Sessoli, M. G. Pini, A. Rettori, M. A. Novak, P. Rosa, M. Massi, M. E. Fedi, L. Giuntini, A. Caneschi, and D. Gatteschi, Phys. Rev. B **72**, 064406 (2005).
[14] C. Coulon, R. Clerac, L. Lecren, W. Wernsdorfer, and H. Miyasaka, Phys. Rev. B **69**, 132408 (2004).
[15] A. Caneschi, D. Gatteschi, N. Lalioti, C. Sangregorio, R. Sessoli, G. Venturi, A. Vindigni, A. Rettori, M. G. Pini, and M. A. Novak, Angew. Chem., Int. Ed. **40**, 1760 (2001).
[16] R. Lescouezec, J. Vaissermann, C. Ruiz-Perez, F. Lloret, R. Carrasco, M. Julve, M. Verdaguer, Y. Dromzee, D. Gatteschi, and W. Wernsdorfer, Angew. Chem., Int. Ed. **42**, 1483 (2003).
[17] T. F. Liu, D. Fu, S. Gao, Y. Z. Zhang, H. L. Sun, G. Su, and Y. J. Liu, J. Am. Chem. Soc. **125**, 13976 (2003).
[18] M. Ferbinteanu, H. Miyasaka, W. Wernsdorfer, K. Nakata, K. Sugiura, M. Yamashita, C. Coulon, and R. Clerac, J. Am. Chem. Soc. **127**, 3090 (2005).
[19] T. Kajiwara, I. Watanabe, Y. Kaneko, S. Takaishi, M. Enomoto, N. Kojima, and M. Yamashita, J. Am. Chem. Soc. **129**, 12360 (2007).
[20] L. M. Toma, R. Lescouezec, J. Pasan, C. Ruiz-Perez, J. Vaissermann, J. Cano, R. Carrasco, W. Wernsdorfer, F. Lloret, and M. Julve, J. Am. Chem. Soc. **128**, 4842 (2006).
[21] H. Miyasaka, T. Madanbashi, K. Sugimoto, Y. Nakazawa, W. Wernsdorfer, K. Sugiura, M. Yamashita, C. Coulon, and R. Clerac, Chem.-Eur. J. **12**, 7029 (2006).
[22] L. Lecren, W. Wernsdorfer, Y. G. Li, A. Vindigni, H. Miyasaka, and R. Clerac, J. Am. Chem. Soc. **129**, 5045 (2007).
[23] R. Clerac, H. Miyasaka, M. Yamashita, and C. Coulon, J. Am. Chem. Soc. **124**, 12837 (2002).
[24] E. Coronado, J. R. Galan-Mascaros, and C. Marti-Gastaldo, J. Am. Chem. Soc. **130**, 14987 (2008).
[25] W. Wernsdorfer, R. Clerac, C. Coulon, L. Lecren, and H. Miyasaka, Phys. Rev. Lett. **95**, 237203 (2005).
[26] P. Gambardella, A. Dallmeyer, K. Maiti, M. C. Malagoli, W. Eberhardt, K. Kern, and C. Carbone, Nature (London) **416**, 301 (2002); P. Gambardella, J. Phys.: Condens. Matter **15**, S2533 (2003).
[27] C. Benelli, A. Caneschi, D. Gatteschi, and R. Sessoli, Inorg. Chem. **32**, 4797 (1993).
[28] J. Villain, Ann. Isr. Phys. Soc. **2**, 565 (1978).
[29] F. Cinti, A. Rettori, M. G. Pini, M. Mariani, E. Micotti, A. Lascialfari, N. Papinutto, A. Amato, A. Caneschi, D. Gatteschi, and M. Affronte, Phys. Rev. Lett. **100**, 057203 (2008).
[30] C. Benelli, A. Caneschi, D. Gatteschi, and R. Sessoli, J. Appl. Phys. **73**, 5333 (1993).
[31] C. Benelli, A. Caneschi, D. Gatteschi, and R. Sessoli, Adv. Mater. **4**, 504 (1992).
[32] L. Bogani, C. Sangregorio, R. Sessoli, and D. Gatteschi, Angew. Chem., Int. Ed. **44**, 5817 (2005).
[33] K. Bernot, L. Bogani, A. Caneschi, D. Gatteschi, and R. Sessoli, J. Am. Chem. Soc. **128**, 7947 (2006); K. Bernot, L. Bogani, R. Sessoli, and D. Gatteschi, Inorg. Chim. Acta **360**, 3807 (2007).
[34] K. Bernot, J. Luzon, L. Bogani, M. Etienne, A. Caneschi, C. Sangregorio, M. Shanmugam, R. Sessoli, D. Gatteschi, J. Am. Chem. Soc. (to be published).
[35] B. O. Roos and P. A. Malmqvist, Phys. Chem. Chem. Phys. **6**, 2919 (2004).
[36] G. Karlström, R. Lindh, P. A. Malmqvist, B. O. Roos, U. Ryde, V. Veryazov, P. O. Widmark, M. Cossi, B. Schimmelpfennig, P. Neogrady, and L. Seijo, Comput. Mater. Sci. **28**, 222 (2003).
[37] B. A. Heß, C. M. Marian, U. Wahlgren, and O. Gropen, Chem. Phys. Lett. **251**, 365 (1996).
[38] F. Aquilante, T. B. Pedersen, and R. Lindh, J. Chem. Phys. **126**, 194106 (2007).
[39] K. Bernot, J. Luzon, R. Sessoli, A. Vindigni, J. Thion, S. Richeter, D. Leclercq, J. Larionova, and A. van der Lee, J. Am. Chem. Soc. **130**, 1619 (2008).
[40] H. Tajima, G. Yoshida, M. Matsuda, K. Nara, K. Kajita, Y. Nishio, N. Hanasaki, T. Naito, and T. Inabe, Phys. Rev. B **78**, 064424 (2008).
[41] R. Pandit and C. Tannous, Phys. Rev. B **28**, 281 (1983).

[42] J. A. Krumhansl and J. R. Schrieffer, Phys. Rev. B **11**, 3535 (1975).

[43] Quite similarly, for a single B-type chain, in the lth unit cell, there are two spins, $\mathbf{S}^{\mathrm{I}}(l)$ and $\mathbf{S}^{\mathrm{II}}(l)$, characterized by two different local axes, $\mathbf{z}'_{\mathrm{I}}$ and $\mathbf{z}'_{\mathrm{II}}$, forming equal angles ($\theta_{\mathrm{I}}=\theta_{\mathrm{II}}=75°$) with the chain axis b, and angles differing by 180° with the a axis within the ac plane. In this case, one has $\phi_{\mathrm{I}}=-45°$, $\phi_{\mathrm{II}}=135°$.

[44] W. H. Press, S. A. Teukolsky, W. T. Vetterling, and B. P. Flannery, *Numerical Recipes in Fortran* (Cambridge University Press, Cambridge, USA, 1986).